

Crystal structures of amyloidogenic segments of human transthyretin

Lorena Saelices , Stuart A. Sievers, Michael R. Sawaya, and David S. Eisenberg*

¹Departments of Biological Chemistry and Chemistry and Biochemistry, Molecular Biology Institute, Box 951570, UCLA, Howard Hughes Medical Institute, UCLA-DOE Institute, Los Angeles, California, 90095-1570

Received 26 January 2018; Accepted 4 April 2018
DOI: 10.1002/pro.3420
Published online 00 Month 2018 proteinscience.org

Abstract: Amyloid diseases are characterized by the deposition of proteins in the form of amyloid fibrils, in organs that eventually fail. The development of effective drug candidates follows from the understanding of the molecular processes that lead to protein aggregation. Here, we study amyloidogenic segments of transthyretin (TTR). TTR is a transporter of thyroxine and retinol in the blood and cerebrospinal fluid. When mutated and/or as a result of aging, TTR aggregates into amyloid fibrils that accumulate in organs such as the heart. Recently, we reported two amyloidogenic segments that drive amyloid aggregation. Here, we report the crystal structure of another six amyloidogenic segments of TTR. We found that the segments from the C-terminal region of TTR form in-register steric-zippers with highly-interdigitated, wet interfaces, whereas the β -strand B from the N-terminal region of TTR forms an out-of-register assembly, previously associated with oligomeric formation. Our results contribute fundamental information for understanding the mechanism of aggregation of TTR.

Keywords: amyloid; transthyretin; steric zipper; out-of-register; amyloidogenic segments; crystallography

Abbreviations: ATTR, transthyretin amyloidosis;; TTR, transthyretin.

Stuart A. Sievers's current address is Kite Pharma Inc, Santa Monica, California.

Grant sponsor: Howard Hughes Medical Institute; Grant sponsor: National Institutes of Health; Grant numbers: AG048120, AG054022, AG029430; Grant sponsor: People Programme (Marie Curie Actions) of the European Union's Seventh Framework Programme (FP7/2007-2013) under Research Executive Agency (REA); Grant number: 298559; Grant sponsor: UCLA-DOE X-ray Crystallography Core Facility is supported by DOE; Grant number: DE-FC02-02ER63421; Grant sponsor: National Center for Research Resources; Grant number: 5P41RR015301-10; Grant sponsor: National Institute of General Medical Sciences; Grant number: 8 P41 GM103403-10; Grant sponsor: National Institutes of Health. Use of the APS is supported by DOE; Grant number: DE-AC02-06CH11357.

*Correspondence to: David S. Eisenberg, D. Phil., Howard Hughes Medical Institute, UCLA-DOE Institute, Departments of Biological Chemistry and Chemistry and Biochemistry, Molecular Biology Institute, Box 951570, UCLA, Los Angeles, California 90095-1570. E-mail: david@mbi.ucla.edu

Introduction

Several pathological conditions, including Alzheimer's disease, Parkinson's diseases, type II diabetes, cardiac amyloidosis, and prion diseases, are associated with the formation of amyloid fibrils and other protein aggregate deposits that result in cytotoxicity and/or mechanical tissue damage.¹ Each amyloid disease is associated with the deposition of particular proteins in the form of elongated, unbranched amyloid fibers. For a long time, treatments for amyloid diseases have been held back by limited information on the structures of the amyloid state of proteins and the causes of aggregation of these disease agents. In recent years, scientists have made incredible progress in this regard. Together with NMR and Cryo-EM reconstruction methods, x-ray crystallography has proven to be a powerful tool for structure determination of proteins in their amyloid state and have notably contributed to the understanding of the molecular architecture of the amyloid spine.

The in-register steric zipper is one of the two main structural motifs that have been identified in amyloid proteins. The spine of amyloid fibrils is made up of pairs of β -sheets, each of which is composed of hundreds of thousands of β -strands stacked along the fibril axis by hydrogen bonding.² This structural arrangement is responsible for the cross- β diffraction pattern that amyloid fibrils display when subjected to an x-ray beam.³ Overall, the spine of the amyloid fibril is made of specific protein segments that are the adhesive parts of amyloid proteins.⁴ The molecular architecture of the amyloid spine has been reproduced by determining the crystal structures of these adhesive segments in their amyloid state.⁵ These structures reveal a motif of a pair of in-register β -sheets whose side chains interdigitate into a steric zipper, forming a dry interface between the two β -sheets.⁴ To date, more than 100 atomic-resolution crystal structures of in-register steric zippers have been determined from over 15 disease-associated amyloid proteins.²

The out-of-register β -sheet is the second structural motif that has been associated with amyloid polymers, and more specifically with oligomeric assemblies. In-register sheets (parallel or antiparallel) are easily recognized in fibrillar assemblies because their strands run perpendicular to the fibril axis. Correspondingly, out-of-register β -sheets are easily recognized in fibrillar assemblies because their strands tilt away from the fibril axis perpendicular, as a result of shearing between strands. Structural details of out-of-register sheets were first revealed for an 11-residue segment of the nonpathogenic amyloid-forming protein, α B-crystallin.⁶ Six copies of the segment stacked in an antiparallel out-of-register β -sheet, which curved into a closed β -barrel with shear number, $S = 6$. Since then, several other out-of-register structures of toxic segments of amyloid proteins have been identified.⁷⁻⁹

Transthyretin (TTR) is a 55-kDa tetrameric protein associated with systemic amyloidoses. In healthy individuals, TTR functions as a hormone transporter that travels in the blood and cerebrospinal fluid.¹⁰ The x-ray structure of the TTR tetramer shows that each identical 127-residue subunit is made of eight β -strands (named A through H) and one α -helix.¹¹ Under pathological conditions, TTR tetramers dissociate and monomers unravel to form amyloid fibrils that deposit in virtually every organ leading to tissue damage, organ failure, and eventual death.¹² Amyloid deposition of mutant and wild-type protein causes hereditary and wild-type TTR amyloidoses (ATTR), respectively. ATTR fibrils comprise full-length TTR and/or C-terminal fragments, indicating that the C-terminus of TTR is essential for amyloid formation.¹³ In a previous study, we showed that the self-association of two segments of TTR from the β strands F and H drive

amyloid fibril formation; however several other segments have the capacity to form amyloid-like fibrils in isolation.¹⁴ We determined the crystal structures of the two amyloid-driving segments in their amyloid states forming in-register steric zippers.¹⁴ Here, we report the crystal structures of six new amyloidogenic segments of TTR in their amyloid state, including a segment that contains a familial mutation associated with early-onset ATTR. In this study, we found the two amyloid structural motifs among them: in-register steric zippers formed by segments from the C-terminal end, and one out-of-register steric zipper formed by an N-terminal segment.

Results

Overall, we have analyzed the amyloidogenicity of thirteen TTR segments predicted to form steric zippers (Fig. 1). These are ¹²LMVKVL¹⁷, ²⁵AINVAV^{27,30}NVAVHV²⁸, ³²VAVHVF³³, ³⁷AADTWE⁴² (carrying the familial mutation ATTR-D38A), ⁴⁷GTKSES⁵², ⁶⁵VEGIYK⁷⁰, ⁶⁸IYKVEI⁷³, ⁸⁰KALGIS⁸⁵, ⁹¹AEVVFT⁹⁶, ¹⁰⁵YTIAAL¹¹⁰, ¹⁰⁶TIAALLS¹¹², and ¹¹⁹TAVVTN¹²⁴. In a previous study, we showed that the segments ¹²LMVKVL¹⁷, ²⁵AINVAV²⁸, ³⁰VAVHVF³³, ⁸⁰KALGIS⁸⁵, ⁹¹AEVVFT⁹⁶, ¹⁰⁵YTIAAL¹¹⁰, ¹⁰⁶TIAALLS¹¹², and ¹¹⁹TAVVTN¹²⁴ can form amyloid-like fibrils in solution, which display a cross- β diffraction pattern when subjected to x-ray.¹⁴ In that study, we also showed that the segments ⁹¹AEVVFT⁹⁶ and ¹¹⁹TAVVTN¹²⁴ drive transthyretin aggregation in vitro by self-association and formation of steric zipper spines of amyloid fibrils. ⁹¹AEVVFT⁹⁶ forms a Class-7 in-register steric zipper in which the β -strands stack in antiparallel equifacial β -sheets, and these sheets in turn pack side-by-side, related by translation. ¹¹⁹TAVVTN¹²⁴ forms a Class-2 in-register steric zipper in which the β -strands stack into parallel β -sheets and the sheets pack face-to-back. Here, we expand our previous work and report the crystal structures of six additional amyloidogenic segments of TTR forming five in-register and one out-of-register steric zippers. Data collection and refinement statistics can be found in Table I. Several distance measurements, buried surface area, shape complementarity, and solvation energy were calculated and can be found in Table II.

The hexameric segment ⁶⁸IYKVEI⁷³ forms a Class 7 steric zipper, in which β -strands stack into antiparallel, equifacial β -sheets, and these sheets pack side-by-side, related by translation [Fig. 2(A)]. The interface is hydrophobic and lacks tight interdigitation. In addition, this steric zipper presents the shortest interface among TTR amyloid structures [Fig. 2(Aii)]; only three side chains (⁶⁸isoleucine, ⁷¹valine, and ⁷³isoleucine) participate in the formation of the hydrophobic interface.

The segment ⁸⁰KALGIS⁸⁵ forms a Class 6 steric zipper, in which β -strands stacked into antiparallel,

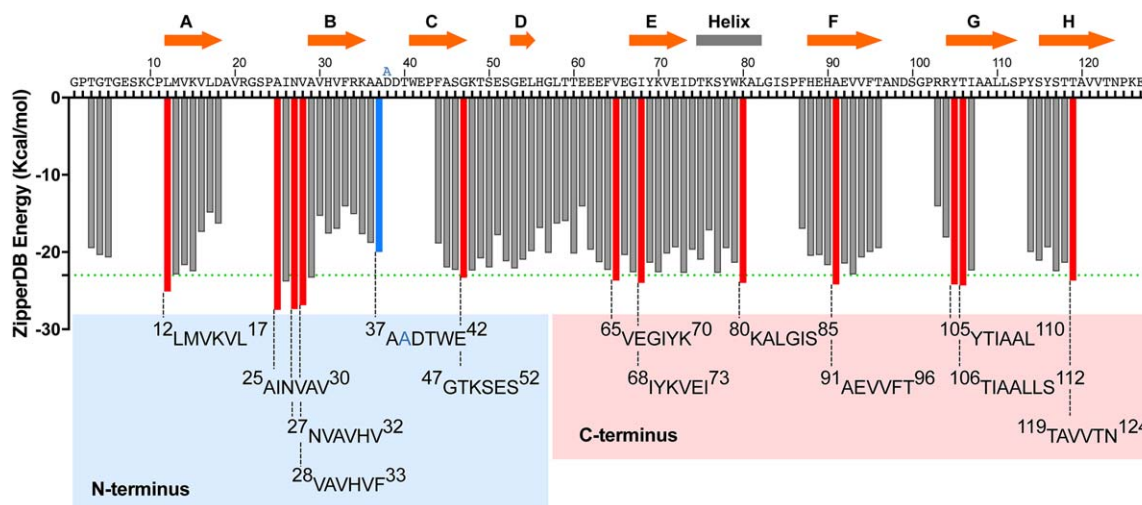


Figure 1. Propensities of steric zipper formation of each 6-residue segment within the TTR sequence. Amyloidogenic propensities were calculated using the 3D profiling method ZipperDB.¹⁵ Segments having energies of $-23 \text{ kcal mol}^{-1}$ (green dashed line) or lower are predicted to form fibrils.¹⁶ Segments that we selected for crystallization are represented with red bars. The segment containing the familial mutation ATTR-D38A is represented with a blue bar. The ZipperDB Rosetta energy prediction of the wild-type sequence ³⁷AADTWE⁴² is $-18.0 \text{ kcal mol}^{-1}$ compared to $-20.0 \text{ kcal mol}^{-1}$ of the mutant sequence ³⁷AADTWE⁴². The schematic of the secondary structure of native TTR is shown on top of the sequence. The blue and pink boxes highlight the TTR segment sequences of the N-terminal and C-terminal regions, respectively, that we described in this study. Only two segments of the N-terminus, ²⁸VAVHVF³³ and ³⁷AADTWE⁴², resulted in the formation of diffracting crystals. From the C-terminus, only the segment ⁶⁵VEGIYK⁷⁰ did not result in a crystal structure.

antifacial β -sheets, and these stack face-to-back [Fig. 2(B)]. The ⁸⁰KALGIS⁸⁵ steric zipper contains a highly hydrophobic interface in which leucines and

isoleucines of one β -sheet interact with alanines and glycines from the opposite β -sheet [Fig. 2(Bii)]. As a result of the structural packing and the short or

Table I. Statistics of Structure Determination of TTR Amyloidogenic Segments

	²⁸ VAVHVF ³³	³⁷ AADTWE ⁴²	⁶⁸ IYKVEI ⁷³	⁸⁰ KALGIS ⁸⁵	¹⁰⁵ YTIAAL ¹¹⁰	¹⁰⁶ TIAALLS ¹¹²
Protein Data Bank Code						
Data collection						
Resolution (Å)	18.37–1.85	21.58–1.00	15.96–1.50	12.57–1.60	22.40–1.60	14.21–1.79
Space group	P2 ₁ 2 ₁ 2 ₁	P2 ₁	P2 ₁	P1	I222	P2 ₁
Unit cell dimensions (Å)						
<i>a</i>	11.53	9.02	9.60	8.06	18.75	9.60
<i>b</i>	20.36	43.16	29.45	9.48	9.56	17.30
<i>c</i>	36.73	9.392	16.03	25.66	44.80	25.00
Unit cell angles (°)						
α	90.00	90.00	90.00	96.35	90.00	90.00
β	90.00	102.84	95.66	96.35	90.00	95.76
γ	90.00	90.00	90.00	110.05	90.00	90.00
Measured reflections	2808	44658	3865	2536	3501	2757
Unique reflections	907	3204	1413	871	625	2692
completeness (%)	82.4 (82.8)	83.5 (46.8)	96.3 (96.7)	95.6 (93.5)	98.9 (99.1)	97.5 (93.4)
<i>R</i> _{merge} (%) ^a	27.8 (43.1)	12.8 (3.97)	15.4 (51.7)	13.8 (67.5)	10.3 (31.8)	21.7 (55.6)
$\langle I/\sigma I \rangle$	5.23 (2.79)	18.43 (5.57)	5.06 (2.08)	5.72 (1.41)	14.22 (5.24)	5.5 (1.8)
Refinement						
Final <i>R</i> _{work} (%) ^b	18.5	11.1	20.5	18.1	20.0	18.7
Final <i>R</i> _{free} (%) ^c	19.7	12.4	26.2	21.2	24.4	22.8
r.m.s.d. bond length (Å)	0.006	0.005	0.008	0.006	0.007	0.014
r.m.s.d. bond angle (°)	0.896	1.264	1.144	1.170	0.896	1.641
Number of protein atoms	102	98	108	82	46	96
Number of ligand/ion atoms	0	0	7	11	0	0
Number of water atoms	4	5	4	2	4	5
Mean B value (Å ²)	5.35	3.311	5.02	9.92	10.22	6.636

Values in parentheses correspond to the highest resolution shell. ^a $R_{\text{merge}} = \sum I_j - \langle I \rangle / \sum I$. ^b $R_{\text{work}} = \sum |F_o - F_c| / \sum F_o$. ^c $R_{\text{free}} = \sum |F_o - F_c| / \sum F_o$ calculated using a random set containing 10% reflections that were not included throughout structure refinement.

Table II. Structural Analytics of TTR Steric Zippers

Peptide sequence	A. Rosetta relax energy (kcal/mol)	B. Distance sheet-sheet \pm S.D. (\AA)	C. Distance strand-strand (\AA)	D. Area buried (\AA^2)	E. Shape Complementarity	F. Solvation Energy
²⁸ VAVHVF ³³	-17.6 (-2.93)	9.7 ± 0.2	4.82	89	0.57	1602
³⁷ AADTWE ⁴²	-16.6 (-2.77)	8.8 ± 0.1	4.70	150	0.75	264
⁶⁸ IYKVEI ⁷³	-23.6 (-3.93)	8.0 ± 0.1	4.80	114	0.77	1839
⁸⁰ KALGIS ⁸⁵	-14.3 (-2.38)	7.7 ± 0.1	4.74	152	0.71	1669
⁹¹ AEVVFT ⁹⁶	-21.4 (-3.57)	9.3 ± 0.5	4.77	131	0.82	1651
¹⁰⁵ YTIAAL ¹¹⁰	-21.2 (-3.53)	9.4 ± 1.0	4.79	131	0.74	1683
¹⁰⁶ TIAALLS ¹¹²	-25.8 (-3.69)	8.7 ± 0.6	4.80	152	0.67	2170
¹¹⁹ TAVVTN ¹²⁴	-17.0 (-2.83)	8.2 ± 0.8	4.75	129	0.87	917

A. Rosetta relax energies calculated from the reported structures by each strand. In parenthesis, average Rosetta relax energies by residue. **B.** Sheet-to-sheet distances are calculated as the average distance between third degree polynomial fits to backbone atoms of opposite β -sheets, which have been projected down the “fibril” axis. The standard deviation is also reported. **C.** Strand-to-strand distance of parallel sheets is given by the corresponding unit cell length. For in-register antiparallel sheets, it is calculated as this unit cell length divided by two. For out-of-register antiparallel sheets, it is taken as an average over stacked backbone atoms of strand n and $n + 2$. **D.** Area buried is calculated as the difference between the solvent accessible surface area of one β -sheet alone and the same β -sheet when is in contact with the opposite β -sheet¹⁷. The average area buried per β -strand is reported. **E.** Shape complementarity values are calculated for interfaces between opposing sheets of ten β -strands each.¹⁸

absent side chains of alanines and glycines, this steric zipper shows limited interdigitation.

The segment ¹⁰⁵YTIAAL¹¹⁰ forms a Class 8 steric zipper, in which β -strands stack into antiparallel,

equifacial β -sheets, and these sheets stack side-by-side, related by a screw axis normal to the sheet face [Fig. 2(C)]. The average distance between opposing sheets, 9.4 \AA , has a large standard

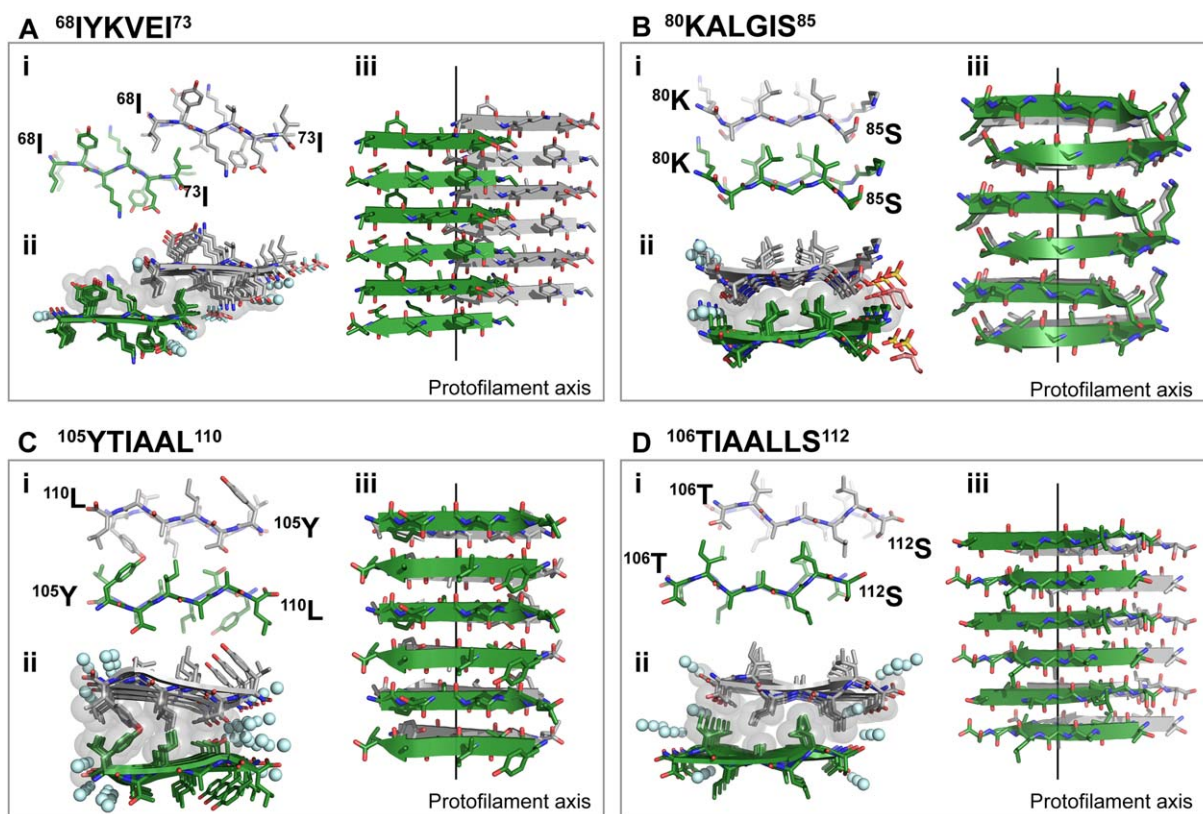


Figure 2. Crystal structures of the amyloidogenic C-terminal segments ⁶⁸IYKVEI⁷³ (A), ⁸⁰KALGIS⁸⁵ (B), ¹⁰⁵YTIAAL¹¹⁰ (C), and ¹⁰⁶TIAALLS¹¹² (D) forming in-register steric zippers. One sheet is shown as dark green; the other is shown as gray. **i.** View down the fibril axis showing two β -strands of each β -sheet in projection. First and last residues of the two top β -strands are labeled. **ii.** View down the fibril axis showing two β -sheets in projection. Water molecules are shown as aquamarine spheres. Gray spheres represent the van der Waals radii of the side chain atoms of the tightly packed fibril core. Other ions present in the crystal are shown as sticks. **iii.** Lateral view of the fibril with the fibril axis indicated by the black line. **i and iii.** Waters and other ligands are not shown for clarity.

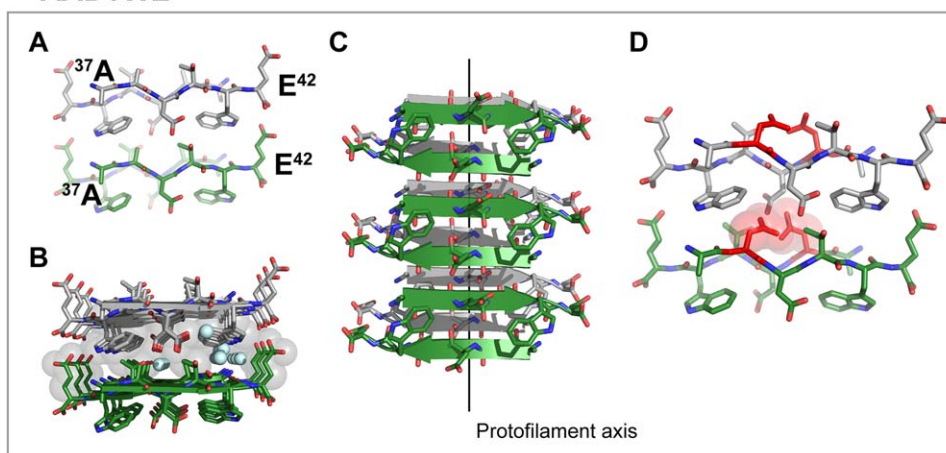


Figure 3. Crystal structure of the in-register steric zipper formed by the amyloidogenic segment ³⁷AADTWE⁴², which carries the familial mutation ATTR-D38A. One sheet is shown as dark green; the other is shown as gray. (A) View down the fibril axis showing two β -strands of each β -sheet in projection. First and last residues of the two top β -strands are labeled. (B) View down the fibril axis showing two β -sheets in projection. Water molecules are shown as aquamarine spheres. Gray spheres represent the van der Waals radii of the side chain atoms of the tightly packed fibril core. (C) Lateral view of the fibril with the fibril axis indicated by the black line. (D) View down of the fibril axis showing that the wild-type sequence ³⁷ADDTWE⁴² would introduce severe steric clashes with ³⁸Aspartate, preventing the formation of this steric zipper. Spheres represent the van der Waals radii of the side chain atoms of ³⁸Aspartate. A, C, and D. Waters molecules are not shown for clarity.

deviation due to the disparate pairing of tyrosines at one edge of the zipper, reaching a maximum distance of 12.6 Å, and alanines at the other edge. Notably, the overlapping segment ¹⁰⁶TIAALLS¹¹² forms a steric zipper with different symmetry—class 6 [Fig. 2(D)].

We also determined the structure of the segment ³⁷AADTWE⁴², containing the familial ATTR-D38A mutation associated with neuropathic and cardiomyopathic ATTR¹⁹ (Fig. 3). This segment forms a class 6 steric zipper in which β -strands stack into antiparallel, antifacial β -sheets, and these sheets stack face-to-back [Fig. 3(A–C)]. In contrast to the other amyloid structures, the steric zipper of ³⁷AADTWE⁴² contains a highly-hydrated interface that includes the polar residues threonine and aspartate [Fig. 3(B)]. We found that the presence of a wild-type aspartate in position 38 would be incompatible with the steric zipper formation [Fig. 3(D)].

Finally, we obtained the structure of ²⁸VAVHVF³³, which corresponds to the B β -strand of TTR (Fig. 4). This segment forms an out-of-register class-5 steric zipper in which β -strands stack into antiparallel, antifacial, out-of-register β -sheets, and these sheets pack face-to-face, through a highly hydrophobic interface exclusively made of valines and no ordered water molecules [Fig. 4(A,B)]. The strands from opposing β -sheets cross at an angle of 115° and β -strands do not run perpendicular to the fibril axis as in in-register steric zippers; instead, the β -strands cross the fibril axis at an angle of 65° from the fibril axis [Fig. 4(C)]. As a result, each

strand within each sheet of ²⁸VAVHVF³³ is out of register by one residue, as shown in Figure 4(D). In contrast to previously reported out of register steric zipper structures^{8,9,28}, ²⁸VAVHVF³³ does not display alternating weak and strong hydrogen-bonding interfaces. Instead, every two strands connect throughout the sheet with the same number of hydrogen bonds [Fig. 4(D)].

Discussion

TTR is an amyloid protein whose aggregation causes transthyretin amyloidosis (ATTR).¹² We have previously shown that TTR contains several amyloidogenic segments that can form amyloid fibrils when incubated in isolation.¹⁴ Here, we expand our earlier efforts with a further structural characterization of amyloidogenic segments of TTR.

Steric zippers from the C-terminus of TTR

Our study provides structural information of the amyloidogenic C-terminal region of TTR, found in the protein deposits of all ATTR patients. Some studies suggest that the spine of an amyloid fibril is made of a single, short, specific adhesive segment of the parental amyloid protein.² However, this is not the case in TTR deposits, which consist of long protein stretches with lengths and composition that depend on pathology.¹³ Westermark and colleagues have identified two types of fibrils among ATTR patients.¹³ Type B fibrils contain full-length TTR and are long, extracellular and highly congophilic. Type A fibrils contain a mixture of full-length and

²⁸VAVHVF³³

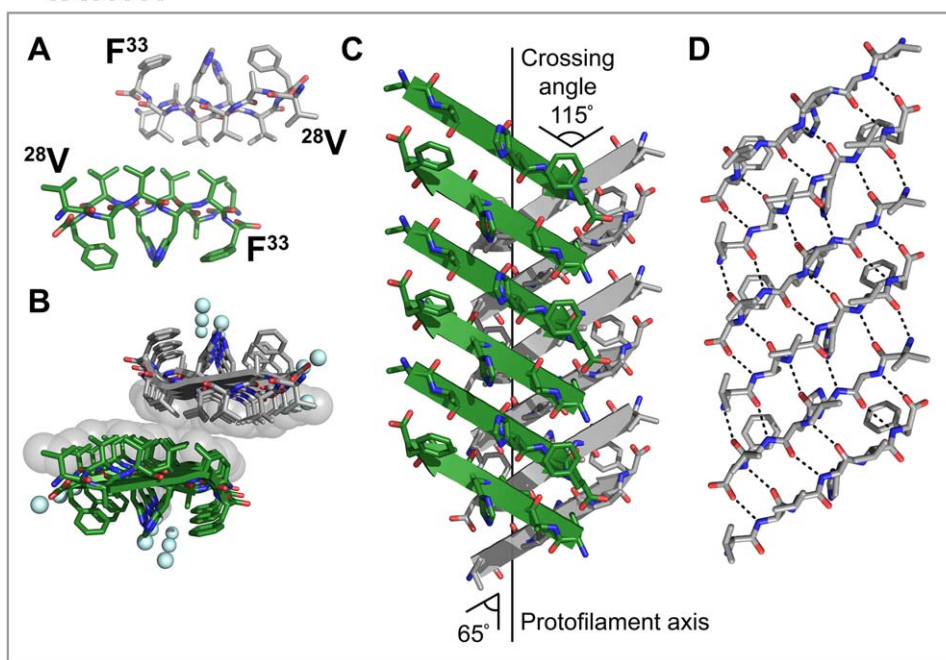


Figure 4. Crystal structure of the out-of-register steric zipper formed by the amyloidogenic segment ²⁸VAVHVF³³. One sheet is shown as dark green; the other is shown as gray. (A) View down the fibril axis showing two β -strands of each β -sheet in projection. First and last residues of the two top β -strands are labeled. (B) View down the fibril axis showing two β -sheets in projection. Water molecules are shown as aquamarine spheres. Spheres represent the van der Waals radii of the side chain atoms of the tightly packed fibril core. (C) Lateral view of the fibril with the fibril axis indicated by the black line. The strands of opposing β -sheets cross at an angle of 115° , 65° to the fibril axis. (D) Intra-sheet hydrogen bonding along one β -sheet. A, C, and D. Waters molecules are not shown for clarity.

truncated C-terminal TTR fragments, and are short and less congophilic. Although we showed that two segments drive TTR aggregation,¹⁴ the presence of C-terminal residues 50 to 127 in both type A and type B ATTR fibrils indicates that this region may be part of the amyloid fibril spine. Our efforts to crystallize TTR segments predicted to form amyloid fibrils included thirteen segments in total, twelve wild-type and one carrying the familial mutation ATTR-D38A. Six of thirteen, including the mutant segment ³⁷AADTWE⁴², are from the N-terminal region of TTR (residues 1 to 50) and seven are from the C-terminal region (residues 50 to 127). We obtained crystal structures from only two segments of the N-terminal region (33%), and one of them was the mutant segment ³⁷AADTWE⁴². In contrast, six C-terminal segments resulted in crystal structures of amyloid-like fibrils (86%), including the two amyloid-driving segments ⁹¹AEVVFT⁹⁶ and ¹¹⁹TAVVTN¹²⁴.¹⁴ They all display the distinctive in-register steric zipper assembly¹⁴ (Fig. 2). The only C-terminal segment that did not crystallize was ⁶⁵VEGIYK⁷⁰, which is the first segment predicted to form amyloid fibrils within the C-terminal stretch and overlaps with ⁶⁸IYKVEI⁷³ that displays a class 7 in-register steric zipper [Fig. 2(A)]. Altogether, 32 residues of the 77 residues of the C-terminus can form amyloid steric zippers, denoting the potential of this region to be involved in the amyloid spine.

Although the sequences of the two segments ¹⁰⁵YTIAAL¹¹⁰ and ¹⁰⁶TIAALLS¹¹² overlap, their amyloid structures reveal different packing and interfaces (Fig. 2). A previous study of this region by NMR described a third structural assembly of a class 4 steric zipper, distinct from class 8 zippers (¹⁰⁵YTIAAL¹¹⁰) and 6 (¹⁰⁶TIAALLS¹¹²) observed by crystallography.²⁰ This structural variability is known as “packing polymorphism,” where the same segment can adopt different steric zipper assemblies.²¹ Similar examples are found in IAPP, associated with type II diabetes,²¹ and amyloid- β and tau, associated with Alzheimer’s disease.^{22,23} The high structural variability of an amyloidogenic segment, such as ¹⁰⁵YTIAALLS¹¹², may be connected to the formation of distinct aggregate subpopulations, and perhaps may play a role in the formation of Type A and Type B fibril subtypes.

Steric zippers from the N-terminus of TTR

We determined the structure of a steric zipper formed by the segment ³⁷AADTWE⁴², containing the familial ATTR-D38A mutation. We have recently found that the amyloid fibrils extracted from the heart of an ATTR-D38A patient were categorized as type B and, therefore, comprise full-length TTR (data not shown). We hypothesize that the mutation ATTR-D38A may create a new steric zipper forming segment since we found that the presence of the

Table III. *Sample Preparation and Crystallization Conditions*

TTR segment	Sample preparation	Crystallization conditions
²⁸ VAVHVF ³³	10 mg/mL in water	0.2 M Magnesium chloride hexahydrate, 0.1 M HEPES sodium pH 7.5, and 30% v/v 2-Propanol
³⁷ AADTWE ⁴²	100 mg/mL in water	0.2 M Ammonium phosphate monobasic, 0.1 M Tris pH 8.5, and 50% v/v MPD
⁶⁸ IYKVEI ⁷³	10 mg/mL in water	1.5 M NaCl, and 10% v/v ethanol
⁸⁰ KALGIS ⁸⁵	10 mg/mL in water	0.1 M Citric acid pH 3.5, and 2.0 M Ammonium sulfate
¹⁰⁵ YTIAAL ¹¹⁰	10 mg/mL in water	100 mM Bis-Tris pH 5.5 and 3 M sodium chloride
¹⁰⁶ TIAALLS ¹¹²	5 mg/mL in 10% acetonitrile	100 mM Tris pH 8.5 and 0.3 M magnesium formate dihydrate

wild-type aspartate in position 38 would be incompatible with the steric zipper formation [Fig. 2(D)]. However, despite its high shape complementarity and large amount of surface area buried, two factors indicative of a strong assembly (Table II), the highly hydrated interface of the steric zipper formed by ³⁷AADTWE⁴² (Fig. 3) and its low solvation energy (Table II) may suggest a weak overall assembly, thereby questioning its implication in fibril formation.

The structural screening of TTR amyloidogenic segments revealed an out-of-register structure formed by ²⁸VAVHVF³³ (Fig. 4). The ²⁸VAVHVF³³ structure differs from the amyloid-like in-register highly-stable structures; it displays the lowest shape complementarity and area buried among the structures of TTR amyloidogenic segments (Table II). Similar to previously determined out-of-register structures, the β -strands of ²⁸VAVHVF³³ cross the protofilament axis at an acute angle.^{8,9} However, in contrast to previous out-of-register structures, each strand of ²⁸VAVHVF³³ participates in equal number of hydrogen bonds ($n = 6$) with strands neighboring either side [Fig. 4(D)], therefore indicating a stable in-sheet packing.

Out-of-register assemblies are associated with amyloid oligomer formation.^{6–8} These sheets show a propensity to curve, likely hindering their ability to form long fibrils, and limiting their growth to oligomeric assemblies. The structure of ²⁸VAVHVF³³ presented here suggests that TTR may be also capable of forming out-of-register oligomers. Although the pathological implications of oligomers in ATTR remains unclear,²⁴ a recent report shows the detection of TTR oligomers in plasma of ATTR patients.²⁵ In that study, Kelly and colleagues generated peptide-based probes that selectively bind TTR oligomers circulating in plasma of polyneuropathic ATTR patients. Interestingly, the probe contains the amyloidogenic segment TTR(25–34) from the β -strand B, with the segment ²⁸VAVHVF³³ as the minimal binding competent sequence. However, they showed that the probe binds C-terminal fragments of TTR that lack the TTR(25–34) segment, indicating that binding of the probe to TTR oligomers must occur through a different region of TTR. Perhaps other segments from the C-terminus may form a

similar out-of-register oligomeric structure that the ²⁸VAVHVF³³ has the ability to recognize.

Conclusions

The present study represents an expansion of the current knowledge on transthyretin aggregation. We have previously shown that the strands F and H drive aggregation of transthyretin by self-association.¹⁴ Here, we show the crystal structures of six additional segments in their amyloid state and describe an antiparallel out-of-register zipper that may be involved in TTR oligomer formation.

Material and Methods

Sample preparation and crystallization conditions

Peptides were synthesized at >97% purity from GenScript (Piscataway, New Jersey) and GL Biochem (Shanghai, China). Peptides were dissolved in water or 10% acetonitrile at a concentration that depended on the solubility of the peptide (Table III). All peptide solutions were spin filtered (0.22 μ m) prior to crystallization experiments at 18°C via hanging-drop vapor diffusion. Crystallizations conditions are detailed in Table III.

Data collection and structure refinement

Data collection and refinement statistics of crystal structures are detailed in Table I. X-ray diffraction data were collected at the Advanced Photon Source beamline 24-ID-E. Molecular replacement was performed with the program Phaser²⁶ using as search models an idealized polyalanine β -strand. Crystallographic refinement was performed using PHENIX,²⁷ REFMAC,²⁸ and BUSTER.²⁹ Model building was performed with Coot³⁰ and illustrated with PyMOL.³¹ The coordinates have been deposited in the Protein Data Bank with accession codes 6C3F, 6C3G, 6C3S, 6C3T, 6C4O, and 6C88.

Structure calculations

Overall energies were calculated from the steric zipper structures by Rosetta Relax.³² Calculations of the area buried and shape complementarity were performed with AREAIMOL¹⁷ and SC,^{18,33} respectively. Area buried was calculated as the difference

in solvent accessible surface area of a central β -strand within the context of a ten-stranded β -sheet and the solvent accessible surface area of the same β -strand in the same ten-stranded sheet in contact with the opposite ten-stranded β -sheet in the zipper. Rosetta energies and shape complementarity were calculated from an assembly made of two opposed β -sheets with ten β -strands each, in the absence of waters or ions. Sheet-to-sheet distances were calculated as the average distance between third degree polynomial fits to backbone atoms of opposing β -sheets, which had been projected down the “fibril” axis. Strand-to-strand distance of parallel sheets is given by the corresponding unit cell length. For in-register antiparallel sheets, it is calculated as this unit cell length divided by two. For out-of-register antiparallel sheets, it is taken as an average over stacked backbone atoms of strand n and $n + 2$.

Conflict of Interests

D.S.E. is an advisor and equity holder of ADRx, Inc. L.S. is a consultant of ADRx, Inc.

Acknowledgments

We thank Glyn Devlin for providing TIAALLS peptide. We thank Duilio Cascio for his assistance with data collection, Michael Collazo of the UCLA Crystallization Facility, the UCLA-Department of Energy (DOE) X-ray Crystallography Core Facility, and M. Capel, K. Rajashankar, N. Sukumar, J. Schuermann, I. Kourinov, and F. Murphy at Northeastern Collaborative Access Team beamline 24-ID-E at the Advanced Photon Source (APS). Data and materials availability: The authors declare that all data generated or analyzed during this study that support the findings are available within this published article and its supplementary information files.

References

- Eisenberg D, Jucker M (2012) The amyloid state of proteins in human diseases. *Cell* 148:1188–1203.
- Eisenberg DS, Sawaya MR (2017) Structural studies of amyloid proteins at the molecular level. *Annu Rev Biochem* 86:69–95.
- Sunde M, Serpell LC, Bartlam M, Fraser PE, Pepys MB, Blake CC (1997) Common core structure of amyloid fibrils by synchrotron X-ray diffraction. *J Mol Biol* 273:729–739.
- Nelson R, Sawaya MR, Balbirnie M, Madsen AO, Riek C, Grothe R, Eisenberg D (2005) Structure of the cross-beta spine of amyloid-like fibrils. *Nature* 435:773–778.
- Sawaya MR, Sambashivan S, Nelson R, Ivanova MI, Sievers SA, Apostol MI, Thompson MJ, Balbirnie M, Wiltzius JJ, McFarlane HT, Madsen AO, Riek C, Eisenberg D (2007) Atomic structures of amyloid cross-beta spines reveal varied steric zippers. *Nature* 447:453–457.
- Laganowsky A, Liu C, Sawaya MR, Whitelegge JP, Park J, Zhao M, Pensalfini A, Soriaga AB, Landau M, Teng PK, Cascio D, Glabe C, Eisenberg D (2012) Atomic view of a toxic amyloid small oligomer. *Science* 335:1228–1231.
- Sangwan S, Zhao A, Adams KL, Jayson CK, Sawaya MR, Guenther EL, Pan AC, Ngo J, Moore DM, Soriaga AB, Do TD, Goldschmidt L, Nelson R, Bowers MT, Koehler CM, Shaw DE, Novitch BG, Eisenberg DS (2017) Atomic structure of a toxic, oligomeric segment of SOD1 linked to amyotrophic lateral sclerosis (ALS). *Proc Natl Acad Sci U S A* 114:8770–8775.
- Liu C, Zhao M, Jiang L, Cheng PN, Park J, Sawaya MR, Pensalfini A, Gou D, Berk AJ, Glabe CG, Nowick J, Eisenberg D (2012) Out-of-register β -sheets suggest a pathway to toxic amyloid aggregates. *Proc Natl Acad Sci U S A* 109:20913–20918.
- Soriaga AB, Sangwan S, Macdonald R, Sawaya MR, Eisenberg D (2016) Crystal structures of IAPP amyloidogenic segments reveal a novel packing motif of out-of-register beta sheets. *J Phys Chem B* 120:5810–5816.
- Ingenbleek Y, Young V (1994) Transthyretin (prealbumin) in health and disease: nutritional implications. *Annu Rev Nutr* 14:495–533.
- Blake CC, Geisow MJ, Oatley SJ, Rerat B, Rerat C (1978) Structure of prealbumin: secondary, tertiary and quaternary interactions determined by Fourier refinement at 1.8 Å. *J Mol Biol* 121:339–356.
- Gertz MA, Benson MD, Dyck PJ, Grogan M, Coelho T, Cruz M, Berk JL, Plante-Bordeneuve V, Schmidt HH, Merlini G (2015) Diagnosis, prognosis, and therapy of transthyretin amyloidosis. *J Am Coll Cardiol* 66:2451–2466.
- Bergstrom J, Gustavsson A, Hellman U, Sletten K, Murphy CL, Weiss DT, Solomon A, Olofsson BO, Westermark P (2005) Amyloid deposits in transthyretin-derived amyloidosis: cleaved transthyretin is associated with distinct amyloid morphology. *J Pathol* 206:224–232.
- Saelices L, Johnson LM, Liang WY, Sawaya MR, Cascio D, Ruchala P, Whitelegge J, Jiang L, Riek R, Eisenberg DS (2015) Uncovering the mechanism of aggregation of human transthyretin. *J Biol Chem* 290:28932–28943.
- Thompson MJ, Sievers SA, Karanicolas J, Ivanova MI, Baker D, Eisenberg D (2006) The 3D profile method for identifying fibril-forming segments of proteins. *Proc Natl Acad Sci U S A* 103:4074–4078.
- Goldschmidt L, Teng PK, Riek R, Eisenberg D (2010) Identifying the amyloids, proteins capable of forming amyloid-like fibrils. *Proc Natl Acad Sci U S A* 107:3487–3492.
- Lee B, Richards FM (1971) The interpretation of protein structures: estimation of static accessibility. *J Mol Biol* 55:379–400.
- Lawrence MC, Colman PM (1993) Shape complementarity at protein/protein interfaces. *J Mol Biol* 234:946–950.
- Kishikawa M, Nakanishi T, Miyazaki A, Shimizu A, Kusaka H, Fukui M, Nishiue T (1999) A new amyloidogenic transthyretin variant, [D38A], detected by electrospray ionization/mass spectrometry. *Amyloid* 6:278–281.
- Fitzpatrick AW, Debelouchina GT, Bayro MJ, Clare DK, Caporini MA, Bajaj VS, Jaroniec CP, Wang L, Ladizhansky V, Müller SA, MacPhee CE, Waudby CA, Mott HR, De Simone A, Knowles TP, Saibil HR, Vendruscolo M, Orlova EV, Griffin RG, Dobson CM (2013) Atomic structure and hierarchical assembly of a cross- β amyloid fibril. *Proc Natl Acad Sci U S A* 110:5468–5473.

21. Wiltzius JJ, Landau M, Nelson R, Sawaya MR, Apostol MI, Goldschmidt L, Soriaga AB, Cascio D, Rajashankar K, Eisenberg D (2009) Molecular mechanisms for protein-encoded inheritance. *Nat Struct Mol Biol* 16:973–978.
22. Colletier JP, Laganowsky A, Landau M, Zhao M, Soriaga AB, Goldschmidt L, Flot D, Cascio D, Sawaya MR, Eisenberg D, (2011) Molecular basis for amyloid-beta polymorphism. *Proc Natl Acad Sci U S A* 108:16938–16943.
23. Seidler PM, Boyer DR, Rodriguez JA, Sawaya MR, Cascio D, Murray K, Gonen T, Eisenberg DS (2018) Structure-based inhibitors of tau aggregation. *Nat Chem* 10:170–176.
24. Manral P, Reixach N (2015) Amyloidogenic and non-amyloidogenic transthyretin variants interact differently with human cardiomyocytes: insights into early events of non-fibrillar tissue damage. *Biosci Rep* 35:e00172.
25. Schonhoft JD, Monteiro C, Plate L, Eisele YS, Kelly JM, Boland D, Parker CG, Cravatt BF, Teruya S, Helmke S, Maurer M, Berk J, Sekijima Y, Novais M, Coelho T, Powers ET, Kelly JW (2017) Peptide probes detect misfolded transthyretin oligomers in plasma of hereditary amyloidosis patients. *Sci Transl Med* 9:eaam7621.
26. McCoy AJ, Grosse-Kunstleve RW, Adams PD, Winn MD, Storoni LC, Read RJ (2007) Phaser crystallographic software. *J Appl Cryst* 40:658–674.
27. Zwart PH, Afonine PV, Grosse-Kunstleve RW, Hung LW, Ioerger TR, McCoy AJ, McKee E, Moriarty NW, Read RJ, Sacchettini JC, Sauter NK, Storoni LC, Terwilliger TC, Adams PD (2008) Automated structure solution with the PHENIX suite. *Methods Mol Biol* 426:419–435.
28. Murshudov GN, Vagin AA, Dodson EJ (1997) Refinement of macromolecular structures by the maximum-likelihood method. *Acta Cryst D* 53:240–255.
29. Blanc E, Roversi P, Vornrhein C, Flensburg C, Lea SM, Bricogne G (2004) Refinement of severely incomplete structures with maximum likelihood in BUSTER-TNT. *Acta Cryst* 60:2210–2221.
30. Emsley P, Cowtan K (2004) Coot: model-building tools for molecular graphics. *Acta Cryst* 60:2126–2132.
31. DeLano WL (2002) PyMOL Molecular Viewer. DeLano Scientific, San Carlos, CA, 700.
32. Conway P, Tyka MD, DiMaio F, Konerding DE, Baker D (2014) Relaxation of backbone bond geometry improves protein energy landscape modeling. *Protein Sci* 23:47–55.
33. Connolly ML (1983) Solvent-accessible surfaces of proteins and nucleic acids. *Science* 221:709–713.